ROBUST DESIGN OPTIMIZATION OF HIGH-PERFORMANCE AXISYMMETRIC SCRAMJETS BASED ON SURROGATE-ASSISTED EVOLUTIONARY ALGORITHMS

A.Saha , T.Ray*, H.Ogawa , R.Boyce**
***Multi-disciplinary Design Optimization Group, University of New South Wales, Canberra,ACT 2600, Australia**
****Centre for Hypersonics, School of Mechanical and Mining Engineering The University of Queensland, Brisbane, QLD 4072, Australia**
A.Saha@student.adfa.edu.au; T.Ray@adfa.edu.au, h.ogawa@@uq.edu.au; r.boyce@uq.edu.au

Keywords: *Scramjet, Robust Design, Optimization, Evolutionary Algorithms*

Abstract

Hypersonic airbreathing engines offer great potential for reliable and economical access-to-space and high-speed atmospheric cruise for both civilian and strategic applications. Scramjet (supersonic combustion ramjet) propulsion, in particular, is a promising technology to materialize efficient and flexible transport systems by removing the need to carry oxidizers and other limitations of rocket engines. In the actual development procedure of aerospace applications, the design for fabrication is carefully determined in consideration of various requirements and criteria, based on the optimal results obtained in numerical analysis and experiments. This stage typically involves a significant amount of engineering activities and human-related factors, which may well give rise to unexpected errors, uncertainty, and accuracy loss in the design values. Discrepancies in the design between the numerical / analytical solutions and the actual product can also arise during operation, originating from various factors such as structural deformation due to aerodynamic loads and surface ablation due to aerothermal heating in hypersonic flight. It is desirable that such discrepancies do not drastically affect the performance of the design. In this work, we present our findings of Multi-objective robust design optimization of the nozzle and external contour of an axisymmetric scramjet. We analyze the effect that uncertainties in the design variables can have on the final solutions and try to understand the behavior from the physical point of view.

1 Introduction

Hypersonic airbreathing engines offer great potential for reliable and economical access-to-space and high-speed atmospheric cruise for both civilian and strategic applications. Scramjet (supersonic combustion ramjet) propulsion, in particular, is a promising technology to materialize efficient and flexible transport systems by removing the need to carry oxidizers and other limitations of rocket engines. A scramjet engine typically consists of an inlet, combustor and a nozzle. During its operation, complex flowfields arise due to highly coupled aerodynamic and aerothermal phenomena including shock/boundary layer interactions, shock/shock interactions and finite-rate chemical reactions.

Design optimization [1] of such complex systems with nonlinear and non-smooth design space represents significant challenges for local-search based optimization methods. Population-based global search via surrogate-assisted evolutionary algorithms coupled with a computational

fluid dynamics (CFD) solver has been found to be highly effective in seeking optima in nonlinear design space in optimization studies conducted at The University of Queensland (UQ) for various axisymmetric scramjet configurations [3, 4, 5], with the main focus on engine performance parameters such as the compression / combustion efficiency and net thrust.

In reality, however, deviations from the intended design can arise during the manufacturing process as well as operation, originating from various factors such as structural deformation due to aerodynamic loads and surface ablation due to aerothermal heating in hypersonic flight. The optimal designs tend to lie at the verge of the border between the feasible and infeasible solutions. In such circumstances minor deviations in design can result in substantial degradation of the performance or critical failure in more severe events. It is therefore of particular importance to select such a design that can maintain desired performance even in the presence of unpredictable disturbances in the design variables.

Robust Design Optimization (RDO) enables the search of optimal solutions that are insensitive to uncertainties inherent in manufacture and operation. It seeks high-performance designs while minimizing the impact of deviations in the design variables on the performance by discouraging such optimal solutions that become highly suboptimal when subjected to minor disturbances. It can thus realize advanced design of enhanced practical use by simultaneously achieving both high performance and robustness.

In this paper, we present the results of an RDO study conducted for a configuration consisting of the nozzle and external contour of an axisymmetric scramjet. The next section describes the original optimization problem [6], followed by the robust optimization procedure in Section 3. The results are discussed and analzed in Section 4, finally conluding the present work in Section 5.

2 Shape optimization of nozzle and external contour

In a recent study, [6], a multi-objective design optimization (MDO) was performed for a configuration consisting of the nozzle and external contour of an axisymmetric scramjet (highlighted in the schematic in Figure 1) for an operating condition at Mach 8 at an altitude of 27 km. In order to achieve both high engine performance and vehicle static stability simultaneously, the study was conducted to minimize the axial position of the centre of gravity normalized by the total length (x_{CG}/L) and maximize the thrust (or minimize the axial force F_x), under the design constraint on the engine volume to allow installation of necessary instrumentation inside.

A distinct Pareto optimal front comprising non-dominated solutions was obtained as a result of the MDO study, clearly indicating the trade-off characteristics between the two objectives, i.e. x_{CG}/L and $-F_x$. Detailed analysis of the optimization results was performed to identify the role and behavior of the individual design variables in achieving the optima. For the purpose of the present study, the non-dominated solutions achieved in optimization for only maximum performance will be referred to as performance-maximizing solutions.

Design optimization is performed in an iterative manner. Fig. 2 schematically shows the optimization chain which consists of mesh generation (pre-processing), CFD computation (evaluation), post-processing and optimization algorithms. Objective functions are evaluated by employing a high-fidelity commercial / research CFD code which solves axisymmetric viscous flowfields involving finite-chemical reactions for the computational mesh that is generated at the pre-processing phase for the geometries represented by a set of the design variables. It is coupled with the MDO capability developed at the University of New South Wales campus at the Australian Defence Force Academy (UNSW@ADFA), based on elitist non-dominated sorting genetic algorithms (NSGA-II) assisted by surrogate modeling.

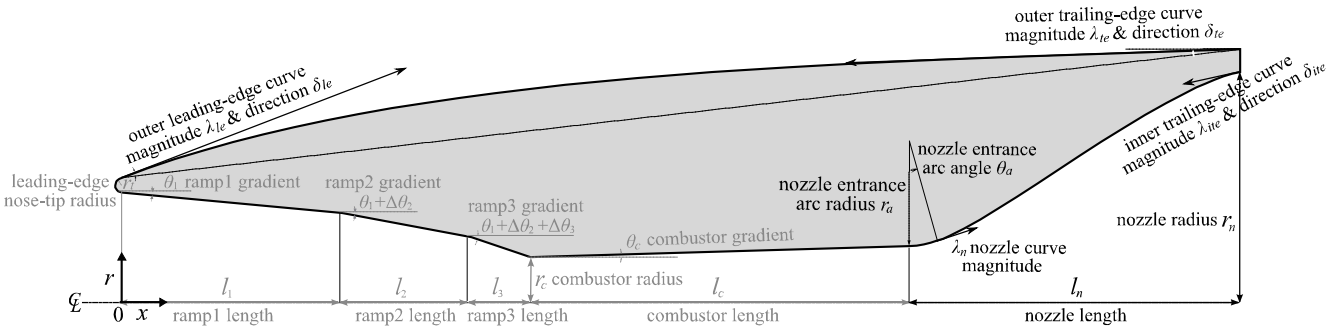

Fig. 1 Parametric representation of an axisymmetric scramjet engine

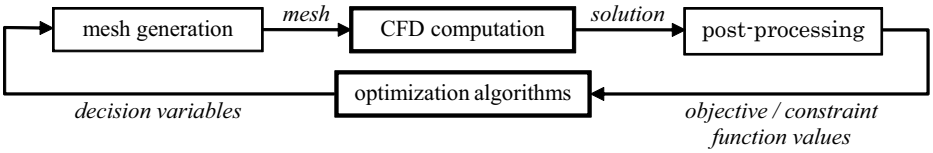

Fig. 2 Optimization loop

3 Robust design optimization

In the actual development procedure of aerospace applications, the design for fabrication is carefully determined in consideration of various requirements and criteria, based on the optimal results obtained in numerical analysis and experiments such as the performance-maximizing solutions described above. This stage typically involves a significant amount of engineering activities and human-related factors, which may well give rise to unexpected errors, uncertainty, and accuracy loss in the design values. Discrepancies in the design between the numerical / analytical solutions and the actual product can also arise during operation, originating from various factors such as structural deformation due to aerodynamic loads and surface ablation due to aerothermal heating in hypersonic flight.

For instance, let us assume here that one of the performance-maximizing non-dominated optimal solutions has been selected for implementation. How would the performance be affected, if the design variables of this solution were perturbed by a meager 1% from the design values ? Would the solution still be feasible ?

A Monte-carlo sampling has been performed in order to investigate the effects of design variable perturbation on the performance by examining 50 neighboring solutions generated by using the Latin Hypercube sampling method, assuming 1% perturbation in the design variables. Figure 3 indicates almost all the solutions have 100% infeasible neighbors that violate one or more geometric constraints, while none violates the volume constraint. Although such a post-optimal analysis of robustness is useful to find the robustness of the obtained solutions, an approach which would be able to directly be able to find the robust solutions would be more useful. Such an approach can be employed in conjunction with existing algorithms in order to realize robust design, which aims to ensure high performance with min-

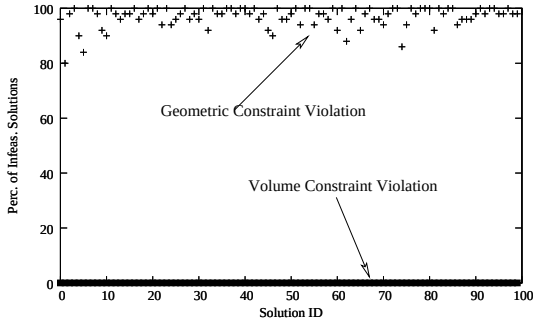

Fig. 3 Percentage of infeasible solutions in the neighborhood of the performance-maximizing non-dominated solutions

imum degradation even in the presence of errors and inaccuracy in the design. Appropriate robustness criteria need to be implemented into the MDO framework to enable the robust design capability. Recently, an EMO procedure for Multi-objective robust optimization, namely, IDEAR was proposed at UNSW@ADFA [2], where the robust design capability was implemented to the advanced MDO capability by improving existing algorithms with respect to the function evaluations to enable economical robust design process. In this procedure designers can specify parameters δ_x and η defined as:

- δ_x: Expected percentage variation in the design variables
- η : Maximum percentage variation allowance in the objective functions

These two parameters are used to enforce additional constraints to the robust design optimization exercise. The first constraint attempts to ensure that the maximum variation in the objective function value is limited by the value of η and is defined as:

$$\max_{i=1,2..,M}\left(\frac{|f_i^*(x)-f_i(x)|}{|f_{i(x)}|}\right)\leq\eta, x\in S \quad (1)$$

where $f^*(x)$ is the mean value of $f(x)$ in the neighborhood of x.

It is interesting to note that with this additional constraint, the designer now has the ability to obtain optimal solutions whose performance measure shall vary by at most a fraction, η under δ_x perturbations in the design space. Smaller the value of η, the smaller the variation of the solutions under the considered uncertainty. It is ofcourse possible, that if the value of η is very small (*tighter* constraint) there may not be any feasible solution in the entire design space for a certain δ_x. However, this information can be easily found out using the above additional constraint with a EMO procedure.

The second constraint attempts to discourage solutions which may be in *feasible islands*, i.e. the solution may be surrounded by a number of infeasible solutions. An immediate implication of this is that solutions on the active constraint boundaries (including side constraints) are not deemed to be robust. IDEAR [2] used a measure, *robust constraint violation* (RCV) of each solution (x), is RCV(x) $=\Sigma_{x^*\in\delta_x}CV(x^*)$, where x^* denotes a solution in the neighborhood of x, denoted by δ_x. The constraint violation of a solution x^* is defined as follows: $CV(x^*)=\Sigma_i g_i(x^*)$, where $g_i(x^*)=0$ if $g_i(x^*)\geq 0$. $g_i(x^*)$ is the value of the i^{th} constraint of the original problem.

To discourage boundary solutions, a penalty term, $GCV(x)$ was added to $RCV(x)$, where $GCV(x)$ is defined as: $GCV(x)=-\Sigma_{x^*\in\delta_x}\Sigma_{i=1}^{N}max\{|v_i(x^*)|,0\}$, where $|v_i(x^*)|$ is absolute violation of i^{th} side constraint. This penalty term could almost negate the possibility of obtaining true optimal solutions as robust solutions, since objective functions of design models often show monotonic behavior and hence the possibility of obtaining boundary solutions as optimal[1]. RCV(x) was hence formulated as follows:

$$\text{RCV(x)}=\Sigma_{x^*\in\delta_x}CV(x^*)+GCV(x^*) \quad (2)$$

Thus, if the robust constraint violation is negative, then at least one of the neighboring solutions was infeasible. The constraint, $RCV(x)$ ensures that a good solution is classified as robust, if it is also feasible in its neighborhood. This is however at best an approximation, since this estimate will depend on the number of neighborhood samples chosen and the technique used to choose the samples. Theoretically, an infinite number of solutions can be generated in the δ_x neighborhood of a solution, x. Hence, a solution x is called a *robust optimal solution*, if it is a Pareto-optimal solution to the following constrained optimization problem in positive null form:

$$\left.\begin{array}{r}\text{Minimize } (f_1(x),f_2(x),..f_M(x)),\\ \text{subject to}\dfrac{\|f^*(x)-f(x)\|}{\|f(x)\|}\leq\eta,\\ RCV(x)\geq 0, x\in S\end{array}\right\} \quad (3)$$

Thus, in the current application, the optimization problem that we solve is:

$$\begin{array}{rl} \text{Min.} & f_1(x) = \frac{X_{CG}}{L}, \\ & f_2(x) = F_x \\ \text{subject to} & V \geq 0.0602\,\text{m}^3, \\ & \frac{\|f^p(x) - f(x)\|}{\|f(x)\|} \leq \eta, \\ & RCV(x) \geq 0, x \in S \\ \text{Where} & \frac{X_{CG}}{L} = \text{Relative C.G position} \\ & \text{normalized by total length} \\ & F_x = \text{Total Axial Force} \end{array} \tag{4}$$

3.1 Quantification of the costs for robust design

Robust non-dominated solutions are commonly found to form a sub-optimal front with respect to the performance-maximizing solutions (to be seen later in Section 4, e.g. Figure 6). This is due to the constraints that have been imposed to achieve the desired robustness specified by the expected variation in the design variables δ_x and maximum variation allowance in the objective functions η. The distance between the Robust optimal front and the performance-maximizing front can be considered as the measure of the sacrifice made for the robustness in terms of the objectives. In order to quantify this a method based on curve fitting has been employed. Firstly the non-dominated solutions on the performance-maximizing front has been approximated by the best fitting polynomial function (in the least-square manner) in the form of

$$F_x = \Sigma_{n=0}^{N_{max}} p_n (x_{CG}/L)^n \tag{5}$$

where the integer N_{max} is varied between 1 and 50 and the best value that can yield the maximum correlation coefficient close to unity is chosen. The best function to approximate the robust non-dominated solutions is then sought by applying an offset x_0 and y_0 in the direction of x_{CG}/L and F_x, respectively, that is,

$$F_x = \Sigma_{n=0}^{N_{max}} p_n (x_{CG}/L - x_0)^n + y_0 \tag{6}$$

where the optimal value set of x_0 and y_0 to minimize root-mean-square (rms) error is found by means of the Nelder-Mead method, starting from the initial point obtained from single-variable minimizations by keeping one offset variable while freezing the other at zero. Displayed in Figure 4 is the variation of the rms error with respect to the offsets x_0 and y_0 for an example case with $\delta_x = 5\%$ and $\eta = 0.5\%$. Compared in Figure 5 are the non-dominated solutions with the approximate curve defined by the polynomial function for the performance-maximizing front and that with the best offsets that have been found in the effort to approximate the robust optimal front. The best offset values x_0=0.0279 and y_0=288N can be interpreted as the price that has been paid in terms of x_{CG}/L and F_x, respectively, in order to fulfill the robustness target of $\delta_x = 5\%$ and $\eta = 0.5\%$ in this case.

In the next section, we present results of solving the above optimization problem using IDEAR.

4 Results

A robust design optimization by means of the IDEAR procedure has been performed for the multi-objective design problem of the axisymmetric scramjet nozzle and external contour described in section 2. We consider an uncertainty of 1% in the design variables and limit the maximum percentage change in the objectives by 0.5%. We use the *Simulated Binary Crossover* (SBX) with $P_c = 0.9$ and $\eta_c = 10$, *Polynomial Mutation* with $P_m = 0.2$ and $\eta_m = 50$ with $\alpha = 0.2$ for all our experiments. A population size of 100 is used and the algorithm is run for 100 generations.

Figure 6 displays the robust non-dominated front achieved as a result of optimization, along with the performance-maximizing front.

Figure 7 shows the percentage of neighboring infeasible solutions obtained by applying the same exercise described in section 3 to the robust non-dominated solutions. It can be seen that very few solutions have infeasible neighbors with respect to both geometric and volume constraints. This result clearly demonstrates IDEAR's capability of finding solutions whose objective func-

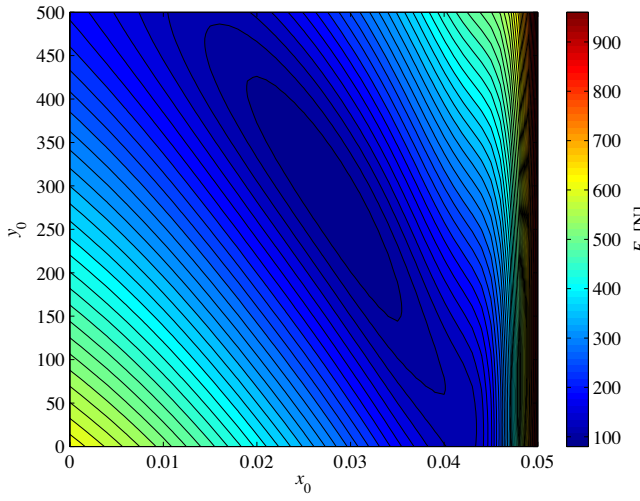

Fig. 4 Variation of the rms error in the approximation of the robust non-dominated solutions with various offsets ($\delta_x = 5\%$ and $\eta = 0.5\%$)

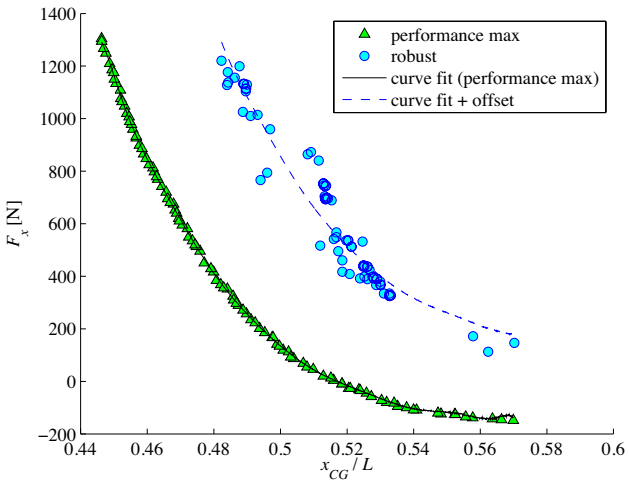

Fig. 5 Non-dominated solutions in comparison with the approximate curves (x_0 = 0.0279 and y_0 = 288N for $\delta_x = 5\%$ and $\eta = 0.5\%$)

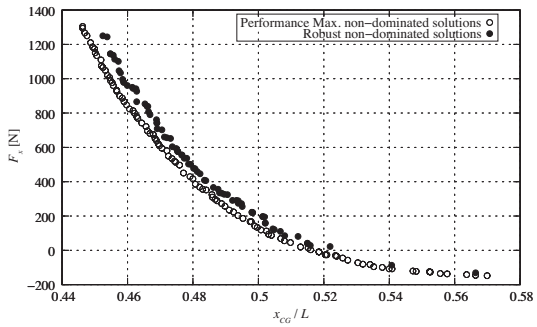

Fig. 6 Robust non-dominated solutions ($\delta_x = 1\%$ and $\eta = 0.5\%$)

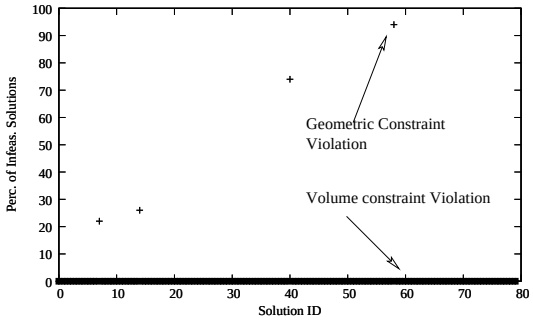

Fig. 7 Percentage of infeasible solutions in the neighborhood of the robust non-dominated solutions

tions are robust against the assumed uncertainty in the design variables. It is also interesting to note that the robust non-dominated solutions form a distinctly sub-optimal front, as compared to the performance-maximizing solutions.

Next, we see how the robust front tends to vary with the value of δ and/or η. Figure 8 shows the fronts for three different combinations of (δ, η). As can be seen that for $\delta = 0.01$, the robust front is slightly sub-optimal as compared to the performance maximizing front for both values of $\eta = 0.005, 0.01$. However, for $\delta = 0.05, \eta = 0.005$, the robust front solutions are highly sub-optimal.

It will be interesting to see the values of the η constraint for the final obtained solutions. Figure 9 shows the value of η for the solutions for two different values of the η constraint (with different δ values as above). As can be seen, the three sets of solutions obey the corresponding η constraints.

4.1 Violation of robust criteria

The distributions plotted in Figure 10 present the degree of the violation for the solutions which have been judged infeasible due to the failure to satisfy the robustness criteria defined in Equation (4), along with the optimal front comprising robust non-dominated solutions displayed for reference. The solutions which are infeasible only because $\triangle\eta < 0$ are represented by square markers whereas the rest of the infeasible solutions unable to fulfill the robustness criteria are denoted by triangles in Figure 10 (a). Similarly the solutions which are infeasible only because of the violation of the constraint for *RCV* are plotted with squares in Figure 10 (b).

The plots in Figure 10 indicate that the solutions infeasible due to the failure to conform to the $\triangle\eta$ robust constraint are characterized with forward relative C.G. positions and intense drag (a), whereas severe violation of the *RCV* criterion is only experienced by infeasible solutions with nearly maximum thrust and rear C.G. positions (b), in concordance with the trends to be observed later in the parallel coordinated plots in

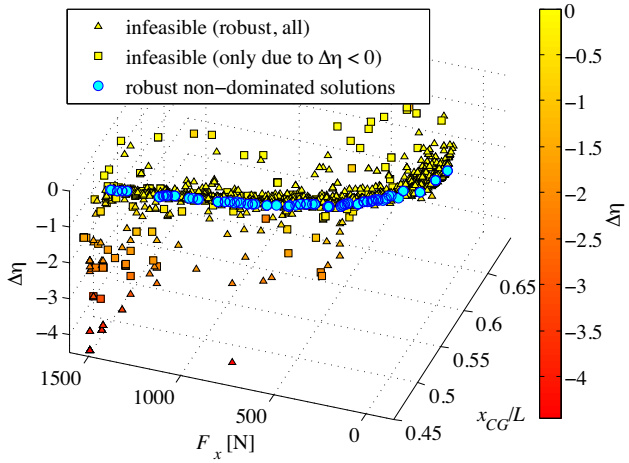

(a) η violation

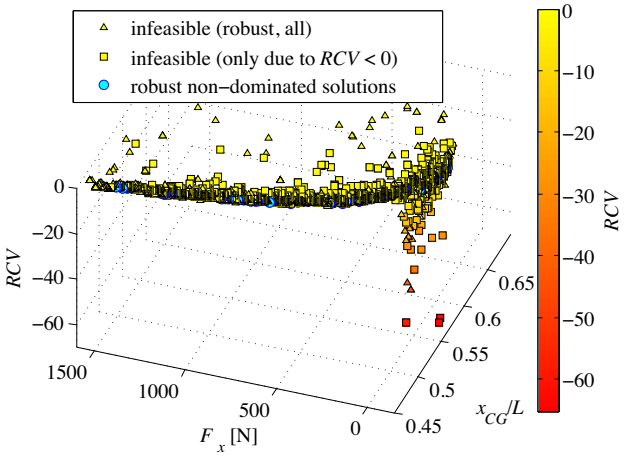

(b) *RCV* violation

Fig. 10 Robust constraint violation of infeasible solutions with respect to the objective functions ($\delta_x = 1\%$ and $\eta = 0.5\%$)

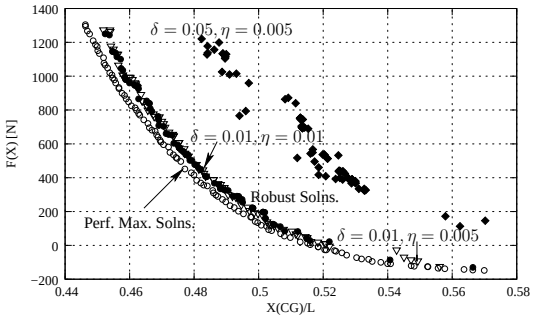

Fig. 8 Robust non-dominated solutions for three sets of (δ and η)

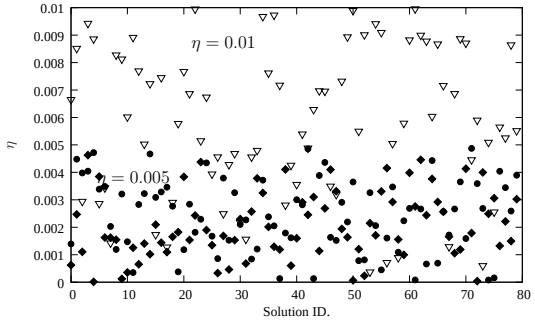

Fig. 9 Value of the η constraint of the Robust Non-dominated solutions ($\eta = 0.5\%, 1\%$)

Figure 12. It is notable that severe violation of the robust criterion mostly occurs against just one of the two robust constraints and simultaneous violation of both robust criteria is a rather minor event (observed mainly near the forward limit of the relative C.G. position in Figure 10 (a)). This behavior of the robust infeasible solutions can be attributed to the exclusive nature of the two robust constraints $\triangle\eta$ and *RCV* plotted in Figure 11, where the vast majority of the robust infeasible solutions lie on the negative side of the either axis ($\triangle\eta = 0$ or $RCV = 0$) with a few off-axis exceptions.

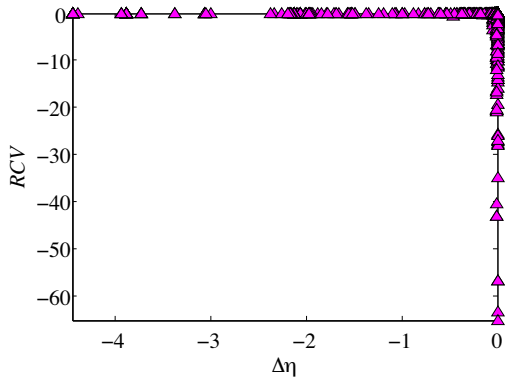

Fig. 11 Distributions of the violation of the robust constraints for infeasible solutions ($\delta_x = 1\%$ and $\eta = 0.5\%$)

4.2 Key parameters for robust design

In order to identify the key parameters which play an important role in robust design, the values of the design variables as well as the objective and constraint functions are visualized in the form of parallel coordinated plots for all the infeasible solutions that have been considered in the course of the optimization over 100 generations for the nominal robust target of $\delta_x = 1\%$ and $\eta = 0.5\%$. In Figure 12 the black lines represent the infeasible solutions that violate the volume constraint $V \geq 0.0602\,\mathrm{m}^3$, while the other solutions represented by lines with colors are infeasible because they satisfy the volume constraint but fail to fulfill either of the robustness constraints described in Equation (4). The colored lines in Figure 12 (a) are the solutions that are infeasible solely because they could not satisfy $\frac{\|f^*(x)-f(x)\|}{\|f(x)\|} \leq \eta$, and the darkness of the lines indicates the degree of violation, that is, the redder the line is, the more severe the violation ($\triangle\eta \equiv \eta - \frac{\|f^*(x)-f(x)\|}{\|f(x)\|}$) is. Similarly the colored lines in Figure 12 (b) represent the solutions considered infeasible due solely to the violation of the RCV constraint ($RCV(x) \geq 0$), whose severity is indicated by the line darkness.

It can be distinctly observed in Figure 12 (a) that the solutions which severely violate the robust constraint for η are characterized by small values of x_{CG}/L close to its minima of 0.45. These forward relative C.G. positions are mainly achieved by altering the forebody contour so that it can possess a front bulge with large values of the leading-edge parameters δ_{le} and λ_{le}, while the nozzle length l_n is maintained near maximum, as also observed in the preceding study [6]. Figure 12 (b), on the other hand, indicates the occurrence of severe violation of the *RCV* criterion

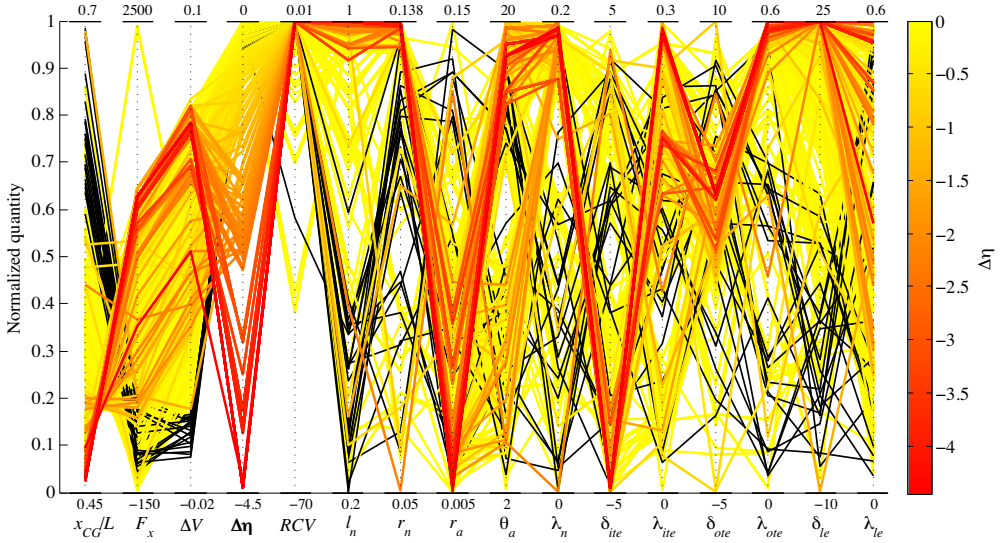

(a) Infeasibility due to η violation

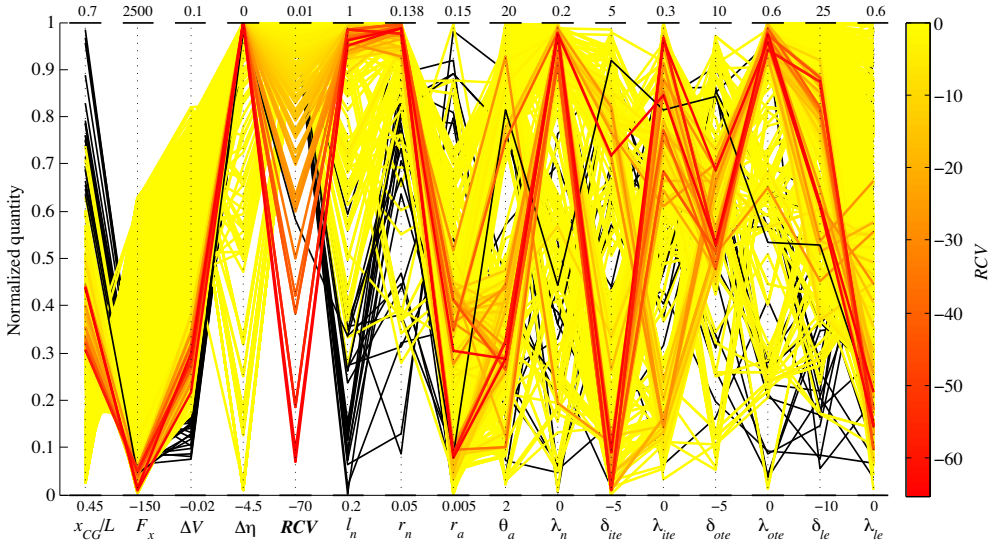

(b) Infeasibility due to *RCV* violation

Fig. 12 Parallel coordinated plots of infeasible solutions for $\delta_x = 1\%$ and $\eta = 0.5\%$ (black lines are infeasible solutions due to violation of the volume constraint, whereas colored lines are infeasible due to robust constraint violation with respect to (a) η and (b) *RCV* constraint)

in the vicinity of the maximum thrust (minimum F_x), which is mainly achieved with favorable nozzle expansion (particularly attained by large nozzle radius r_n) and rather straight external surface (small leading-edge angle δ_{le}), as has also been formerly reported (please refer to [6] for detailed flow analysis).

The following significant implications for robust design can be derived from the results described above in conjunction with the observations made in Section 4.1:

1) The solutions which offer appreciable thrust near the maximum limit (lowest F_x) are susceptible to disturbances in the design variables and tend to result in infeasible solutions that violate the constraint of the original problem, i.e. $V \geq 0.0602\,\mathrm{m}^3$.

2) Deviations in the design variables from the intended values can significantly deteriorate the performance in either of both of the objective functions, i.e. x_{CG}/L and F_x for the solutions with favorable stability characteristics (forward relative C.G. positions).

4.3 Sensitivity analysis

Variance-based global sensitivity analysis [7] has been performed in order to investigate the influence of each design variable x_i (input) on the objective and constraint functions (output). The sensitivity indices are calculated for the input matrices comprising 10,000 (base sample number) rows of 11 columns composed of the decision variables and output vectors obtained from the surrogate model with the best prediction accuracy. The first-order sensitivity indices are plotted for the violation of the *RCV* criterion[1] in Figure 13.

The proportions are characterized by the strong impact of the forebody parameters δ_{le} and λ_{le}, similarly to the trends observed in the sensitivity for x_{CG}/L, F_x and $\triangle V$ in the performance-maximizing optimization (displayed in Figures 26, 27 and 28, respectively, in [6]), while the influence of the nozzle parameters is somewhat increased in the case of *RCV*. This result suggests that particular attention ought to be paid to these influential design parameters in order to prevent the occurrence of *RCV* violation, where the volume criterion is not satisfied by at least one of the neighboring solutions. The similarity found in the sensitivity indices is unsurprising in consideration of the distributions of the robust infeasible solutions due to *RCV* violation, which cluster at the verge of the maximum thrust limit (Figure 10 (b)).

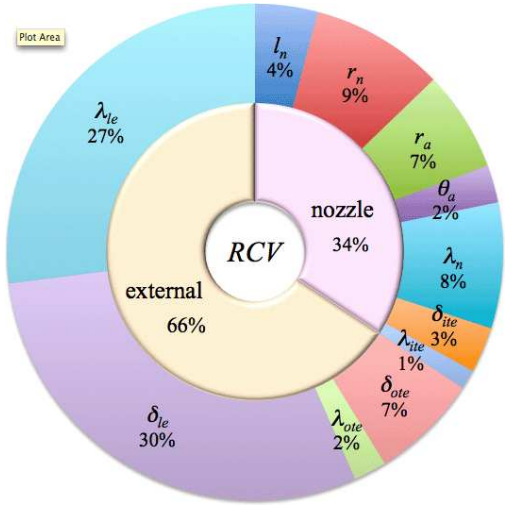

Fig. 13 First-order sensitivity of *RCV* ($\delta_x = 1\%$ and $\eta = 0.5\%$)

The costs that must be paid in the objectives to achieve the desired robustness are quantified by the method outlined in Section 3.1 and tabulated in Table 1 for the δ_x and η values examined in this paper ($\triangle x_{CG}/L = x_0$ and $\triangle F_x = y_0$). It can be noted that the price is rather minor for such moderate robustness requirements as (δ_x, η) = (1%, 0.5%) and (1%, 1%) and must be paid in the form of either objective (δ_x, η) or in combination of both. However, a more stringent requirement in the robustness anticipating an amplified variation ($\delta_x = 5\%$) incurs substantial penalty to be paid in both objectives.

[1] No valid indices have been obtained for $\delta\eta$, which suggests the difficulty in correlating the design variables and the violation of the η criterion.

Table 1 Costs paid in the objectives to achieve various robustness targets

δ_x	η	$\triangle x_{CG}/L$	$\triangle F_x$ [N]
1%	0.5%	0.00299	19.4
1%	1%	0.00495	0
5%	0.5%	0.0279	288

5 Conclusions and Future Work

This paper presents our preliminary investigation into the robust design optimization of an axisymmetric scramjet nozzle and external contour in the presence of an assumed uncertainty in the design variables. It has been found that designs aiming at the maximum attainable thrust tend to incur abrupt decrease in the volume when the design variables deviate from their intended values, thus leading to infeasible geometries. On the other hand, care must be taken for designs targeting superior static stability with forward C.G. because disturbances in the design variables can result in significant penalty in either or both objective functions, that is, the total axial force and forward C.G. positioning itself.

An immediate future goal of our work would be enhance the optimization algorithm to be able to consider different values of deviations in the design variables and objective specific value of the robustness constraint. We also plan to carry out the robust design optimization study on some of our earlier optimization studies such as that of the Inlet geometry and Full-flow path.

References

[1] Papalambros, P., and Wilde, D. *Principles of optimal design: modeling and computation*, Cambridge University Press, 2000.

[2] Saha, A. and Ray, T. *Practical Robust Design Optimization Using Evolutionary Algorithms*, Journal of Mechanical Design ASME

[3] Ogawa, H., and Boyce, R. R. *"Physical Insight into Scramjet Inlet Behaviour via Multi-Objective Design Optimisation"*, in press, *AIAA Journal*.

[4] Ogawa, H., and Boyce, R. R. *"Physical Insight into Nozzle Flow Behaviour of Axisymmetric Scramjets for Access-to-Space via Design Optimisation"*, Proceedings of 10th Australian Space Science Conference, Brisbane, Australia, Sep 2010.

[5] Ogawa, H., Alazet, Y., Pudsey, A., Boyce, R. R., Isaacs, A., and Ray, T., *"Full Flow-Path Optimization of Axisymmetric Scramjet Engines"*, AIAA-2011-2347, 17th AIAA International Space Planes and Hypersonice Systems and Technologies Conference San Francisco, CA, Apr 2011.

[6] Ogawa, H., Brown, L., Boyce, R. R., and Ray, T. *"Multi-objective Design Optimization of Axisymmetric Scramjet Nozzle and External Components Considering Static Stability By Using Surrogate-Assisted Evolutionary Algorithms"*, ISABE-2011-1513, 20th International Society of Airbreathing Engines, Göteborg, Sweden, Sep 2011.

[7] Saltelli, A., Ratto, M., Andres, T., Campolongo, F., Cariboni, J., Gatelli, D., Saisana, M., and Tarantola, S. "*Global Sensitivity Analysis: The Primer*", Wiley-Interscience, Hoboken, NJ, 2008.

5.1 Copyright Statement